Scientiae Radices, **2**(2), 93-111 (2023)

Review

SciRad SCIENTIAE RADICES

Quantum dots for temperature sensing

Natalia Doskaliuk[(1)], Yuliana Lukan[(2)], Yuriy Khalavka[(1)]✉

[(1)] Department of Chemistry and Expertise of Food Products, Yuriy Fedkovych Chernivtsi National University, Ukraine

[(2)] Department of Medical and Pharmaceutical Chemistry Bukovynian State Medical University, Ukraine

✉ Correspondence to: y.khalavka@chnu.edu.ua

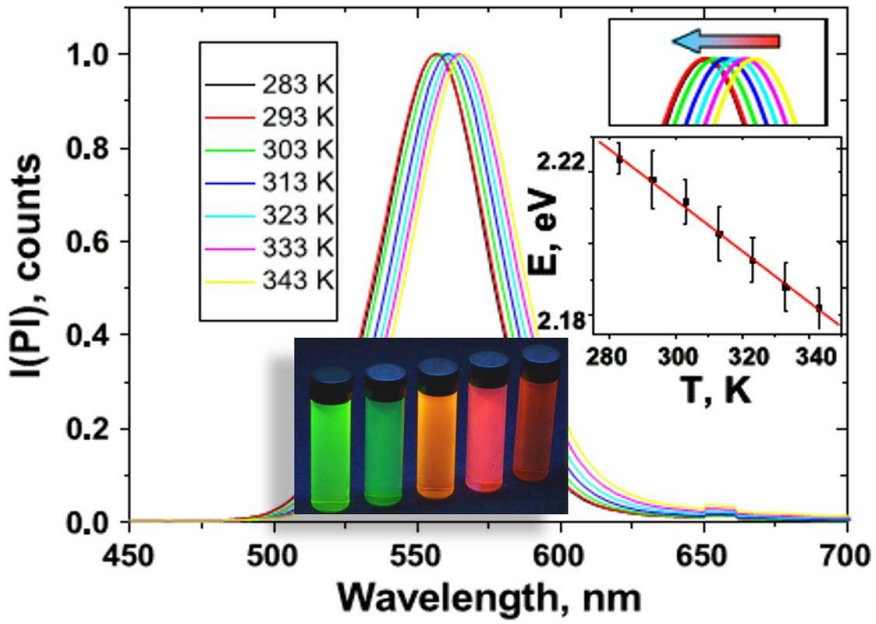

Abstract: Quantum dots are three-dimensional nanoparticles of semiconductors with typical sizes ranging from 2 to 10 nm. Due to the quantum confinement effect the energy gap increase with the size decreasing resulting in size-depended and fine-tunable optical characteristics. Besides this, the energy structure of a quantum dot with a certain size is highly sensitive to environmental conditions. These specific properties open a wide range of applications starting from optical and optoelectronic devices and ending with biosensing and life science. Temperature is one of those parameters influencing strongly on the optical properties of semiconductor nanocrystals, which make them promising materials for temperature sensing, more often using a fluorescent response. Compared to the conventional organic dyes

already applied in this field, quantum dots exhibit a set of advantages, such as high quantum yield and photostability, long fluorescence lifetime, higher Stokes shift, and ability to surface functionalization with targeted organic molecules aimed to provide them biocompatibility. In this review, we briefly discuss the properties of II-VI and assumingly less toxic I-III-VI quantum dots, mechanisms of temperature-induced fluorescence response, and the feasibility of their practical application in the field of thermal sensing.

Keywords: Quantum Dots, Photoluminescence, Thermal Sensing, Temperature Sensitivity, II-VI Semiconductors, I-III-VI Semiconductors, CdTe, CdS, PbS, $AgInS_2$, $CuInS_2$.

Received: 2023.02.24
Accepted: 2023.03.15
Published: 2023.04.19
DOI: 10.58332/scirad2023v2i2a01

Introduction

Semiconductor nanoparticles (NPs) of rather a small size or quantum dots (QDs) have optical properties that determine by quantum confinement, which causes a shift in the energy of the optical transition with the size of the crystal. Such nanomaterials have attracted considerable attention after the development of synthetic procedures allowed to prepare highly monodisperse, well-stabilized, and intensively emitting QDs [1-3].

QDs possess well-pronounced photoluminescence (PL) properties, namely higher luminescence quantum yields (approaching 90% for CdS and InP QDs), narrower wavelength distribution of the emission spectra, and less photobleaching compared to other types of fluorescent probes [4,5].

The synthesis procedures as well as the energy structure determining absorption and Pl mechanisms in II-VI QDs are well developed and understood [6-9], therefore these NPs are already used as a good down-conversion material of LEDs [10], photodetectors [11], catalysts [12], in photovoltaics [13] and bioimaging [14]. However, the heavy metals included in their composition concern one about carcinogenicity and other chronic health risks, as well as disposal hazards. Therefore, Cd-, Hg- and Pb-free I-III-VI NPs, such as $CuInS_2$ (CIS), $AgInS_2$ (AIS), and their alloys and core/shell structures with Zn (ZCIS and ZAIS respectively) were developed [15-18] and proposed as a green alternative in WLEDs [19-21], photocatalysis [22] and biomedical application [23,24]. These ternary QDs with a defined size and size distribution are usually synthesized in colloidal solutions through the hot-injection method, which provides an opportunity to control the growth rate and the formation of nuclei resulting in highly monodisperse material [25,26]. Both aqueous and

organic media are suitable for CIS and AIS NPs preparation, however, it is obvious that water as a dispersant is preferable. In addition, QDs synthesized in an aqueous medium do not require further phase transfer and purification, which allows the avoidance of additional synthetic steps and energy consumption.

The I–III–VI QDs are direct-band semiconductors (E_g near 1.87 eV) with a high absorption coefficient and widely tunable Pl spectral window covering the visible and near-infrared (NIR) regions [24,27,28]. However, the origin and mechanism of the Pl of these NPs are still under discussion. Because of the absence of absorption peak, broad Pl spectra, and large Stokes shift (even as for QDs), it was suggested that their PL does not caused by exciton recombination (apart from II-VI QDs), but by recombination of carriers trapped with intragap levels formed by native point defects [29]. In general, ternary semiconductors are known to be able to accumulate intrinsic point defects due to the presence of two cations of different sizes and low energy of defects formation. The point is that the nature and concentration of defects in ternary QDs, as well as the nature and position of energy levels involved in the carrier's recombination pathway depend on the composition of these materials. However, even with the absence of excitonic emission, these nanomaterials exhibit a noticeable Pl response to temperature fluctuations, making them a promising alternative to more toxic II-VI QDs in the field of temperature sensing.

Discussion

Mechanisms of temperature response of II-VI quantum dots fluorescence

Due to the direct band gap and excitonic type of emission luminescence properties of II-VI QDs are highly sensitive to temperature fluctuation making them promising materials for online (one pot, in-situ) local noncontact thermal monitoring. The QDs band gap energy decreases with temperature increasing shifting the absorption and photoluminescence (Pl) maximum to the red spectral region [30-32]. Besides this, the Pl intensity decreases notably with temperature rise giving additional instruments for thermal sensing [33]. For temperatures slightly higher than the Debye temperature of the material (150 – 170 K for most of the II-VI semiconductors) this effect is associated mainly with exciton-phonon coupling affected by quantum confinement effect [34]. The temperature dependence of the Pl maximum followed by the band gap energy trend and can be fit well with the empirical Varshni equation [35]:

$$E_g(T) = E_{g0} - \alpha \frac{T^2}{T + \beta} \quad (1)$$

where E_{g0} is the band gap energy at 0 K, β is Debye temperature of the material and α is the temperature sensitivity coefficient. Its analytical expression includes the effects of exciton-phonon coupling, quantum confinement, and thermal strain arising from the lattice thermal expansion and pressure of thermally expanded surrounding media [36]:

$$\alpha_{nano} = a_{bulk} + 2k_b(S_{nano} - S_{bulk}) + \frac{h^2\pi^2}{\mu R_{ave}^2}\beta + \left(\frac{\partial E_g}{\partial P}\right)[3B_0(\beta_{env} - \beta)] \quad (2)$$

where α_{bulk} is the temperature coefficient of bulk semiconductor, S_{nano} and S_{bulk} is the Huang–Rhys factors for nanoscale and bulk semiconductor respectively, k_b is the Boltzmann constant, R_{ave} is the QDs average radius, μ is the reduced mass of the electron and hole, h is the Planck's constant, β is the QDs temperature expansion coefficient, $\partial E_g/\partial P$ is a band gap variation due to changes in lattice pressure, B_0 is the bulk modulus and β_{env} is the environment thermal expansion coefficient.

Eq. 2 gives us a very important conclusion: the smallest QDs with the highest thermal expansion coefficient should possess the highest temperature sensitivity. It has been practically confirmed α inversely proportional to the QDs size making the smaller QDs more sensitive to temperature changes [36-38].

Increase of the Pl full width at the half maximum (FWHM) with temperature rise caused by both exciton-acoustic phonon and exciton-longitudinal optical phonon (LO) coupling while in temperature quenching of Pl (decrease of the Pl intensity) together with the thermal escape of carriers due to exciton-LO phonons coupling thermally activated nonradiative processes like surface/interface trapping plays an important role. Because the smaller QDs have a larger amount of surface traps due to a larger specific surface area they should also possess better Pl intensity-based sensitivity. The time-resolved measurement can also provide an instrument for QDs-based temperature sensing. Murphy *et al.* [39] proposed to consider the temperature dependence of the exited carriers' decay rate in terms of transition between a ground state and two excited states: a lower energy dark exciton state and a higher energy bright exciton state including the effect of carrier capturing by external trap states.

In accordance with the selected temperature-depended property of QDs, there distinguish the next approaches to temperature measurement: "intensity luminescence thermometry", "spectral position luminescence thermometry", and "lifetime luminescence thermometry". Nanothermometry can bring significant benefits in such area as micro/nano-electronics, integrated photonics and biomedicine [40]. In principle changes in FWHM could also be used for sensing, but this approach is impractical due to the low magnitude of temperature induced broadening and domination of inhomogeneous type of broadening (caused by size and shape variation).

In the first case, QDs nano thermometers can provide the high-resolution temperature profile obtaining and detecting critically undesirable "hot spots" in microdevices that arise from local unpredictable resistance variation of very small conducting channels. Similarly to that getting knowledge of temperature singularities in integrated photonic devices is very important to provide its correct work taking into account the strong temperature dependence of the optical properties of their functional materials. Finally, many dynamic properties of biological systems (for example cell division rate and the rate of tissue growth) as well as optical and structural properties of biomolecules are highly sensitive to even small temperature variations. From an applied point of view nanothermometry is a very promising technic to detect cancer at an early stage when the number of cancer cells is about a thousand and the size of the tumor is yet invisible to traditional diagnostic methods (about 1 mm). Using QDs nanothermometers in biomedicine has an important advantage – they can be used within the biological optical window which provides the capability of deep tissue imaging.

II-VI QDs intensity luminescence thermometry

One of the earliest research exhibiting the principle of intensity luminescence thermometry was carried out by Walker *et al*. [41]. It demonstrated an appreciable, linear, and reversible (-1.3% per °C) change in Pl intensity of CdSe/ZnS QDs in poly(lauryl methacrylate) matrices for temperatures close to ambient conditions (250–315 K). In that narrow temperature range, the change of the other Pl parameters (blue shift of the emission band maximum and band narrowing) is negligible making the Pl intensity a preferential instrument for temperature deduction.

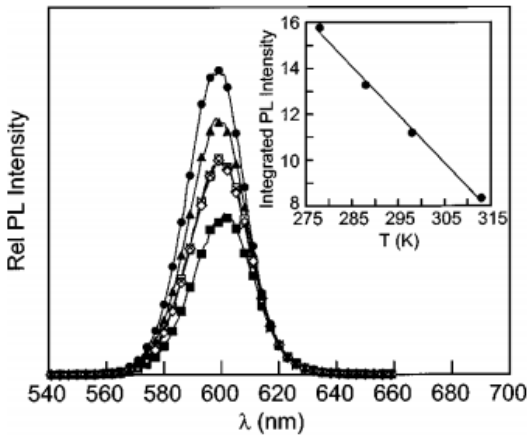

Fig. 1. Pl spectra of CdSe/ZnS QDs in poly(lauryl methacrylate) matrices at different temperatures; insert – temperature dependence of the integrated Pl intensity [41].

The great feasibility of this approach in spatiotemporally varying temperature fields relevant to hyperthermic thermal therapies was demonstrated by Han *et al*. [42]. Two types of CdSe/ZnS with Pl wavelength 620 and 665 were used to obtain the thermal images of human prostate cancer cells. At first, the quantitative imaging of the Pl QDs intensity change was obtained (Fig. 2a), and its intensity–temperature correlation in the range 10–70 ^{0}C was established via creating a temperature gradient of 5 ^{0}C/mm by thermoelectric module and obtaining the temperature profile (Fig. 2b).

Then the cancer cells were incubated with CdSe/ZnS QDs and gold nanoparticles as a mediator of the heating procedure by excitation of plasmon resonance in it. The experimental setup for QD-mediated thermal imaging included the halogen lamp with blue additive filter (transmission wavelength less than 525 nm) to excite the QDs Pl, the NIR 810 nm diode laser for plasmon resonance excitation, and the CCD camera with red additive filter (transmission wavelength more than 600 nm) connected with computer via a frame grabber. The heating of labeled cancer cells was carried out by a short laser beam excitation and the spatiotemporal thermal images with different time spots were obtained (Fig. 2c). The intensity-temperature conversion was conducted using a previously obtained empirical equation with the pre-determined calibration constants. Interesting that QDs with the shorter emission wavelength (most likely due to the smaller size) exhibited better temperature sensitivity because of the above-discussed reasons.

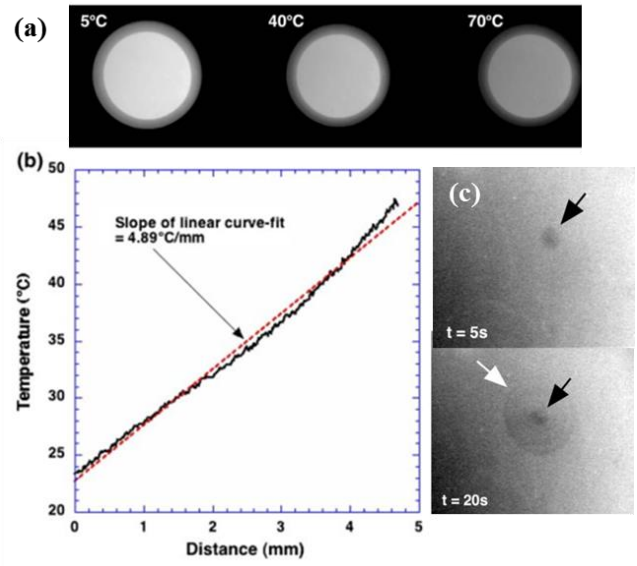

Fig. 2. a) Fluorescence images of QD620 slide with different temperatures; b) QD fluorescence intensity change in a spatial temperature gradient; c) QD fluorescence images of cancer cells during cold nanoparticles mediated heating. QD fluorescence at the spot where the laser was focused decreases, and the dark spot grows in the radial direction with time [42].

It should be noted that the high sensitivity of Pl intensity to the other environmental conditions (surface state of QDs, their concentration, pH of media or chemical presented as well as device/mode features e.g. power of the excitation source, photodetector sensitivity, integration time) requires a careful calibration of the temperature sensing system and make this approach more relevant for the relative assessment of temperature change. From this point of view, the wavelength (energy) of Pl maximum is the more acceptable parameter for temperature measurement and monitoring.

II-VI QDs spectral position thermometry

This approach is based on a linear relationship between temperature and Pl maximum spectral position in the temperature range above Debye temperature.

Several works demonstrate the great capability to determine and map the temperature in nanoscale biological systems and optoelectronic devices via QDs Pl maximum shift [43-45]. The first results of QDs used as nanothermometers for high-resolution fluorescence thermal imaging were obtained by Maestro *et al.* [43]. The human carcinoma cells were incubated with the CdSe QD nanothermometers and imaged by two-photon fluorescence microscopy. The cell temperature was varied by micro-air-heater and a clear red shift of the QDs emission band was observed.

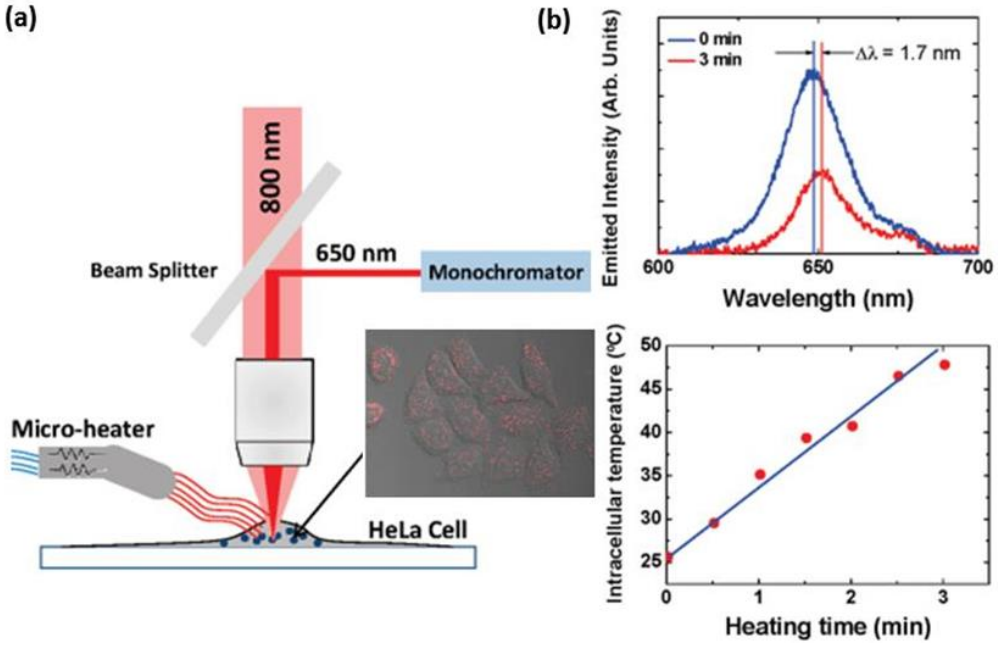

Fig. 3. a) Schematic image of the experimental setup used to measure intracellular temperature through two-photon CdSe-QDs fluorescence; b) Two-photon fluorescence spectra of CdSe-QDs incorporated in a HeLa cell for two different temperatures (top); the intracellular temperature deduced from the spectral shift of the CdSe QDs emission obtained for different heating time (bottom); insert - two-photon excited fluorescence images of HeLa cells (superimposed with optical transmission images) [43].

Using a calibration graph and recording the two-photon excited emission for different heating times authors measured intracellular temperature in real-time (Fig. 3). It has been demonstrated that two-photon excitation leads to a larger spatial resolution due to its nonlinear nature and provides better temperature sensitivity resulting in higher quality thermal images. Li *et al.* [46] demonstrated the local noncontact temperature measurement of a micro-heater on aluminum microwire using Pl shift of individual CdSe QDs. They observed the variation of Pl peak position from dot to dot due to their size, shape, and composition distribution giving a deviation of 2.4 nm for 71 QDs. Using the bootstrap statistical analysis they found the number of particles needed to achieve a certain precision in optical temperature readout. For example to achieve 1 °C precision it should be taken about 1200 particles that require a surface area of ~355 nm in diameter to accommodate these particles (taking into account the presence of polymer layer and streptavidin on CdSe QDs surface).

As mentioned above, the spectral sensitivity of quantum dots turns out to be size dependent. In some cases, Pl color changes can be seen by the naked eye. Fig. 4 shows a typical shift of the emission spectrum for CdTe nanoparticles and Fig. 5 shows the size dependence of the sensitivity. Spectral thermal sensitivity reaches values up to 1,2 meV/K.

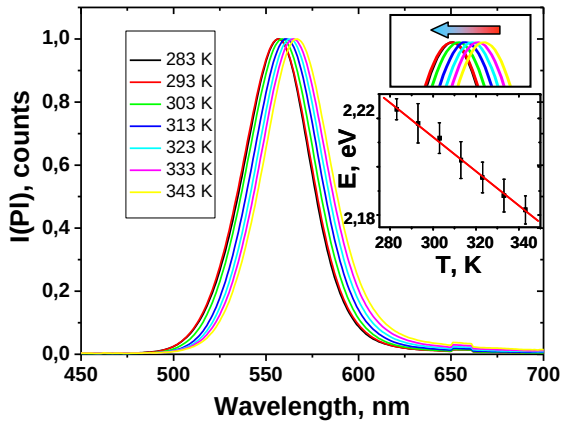

Fig. 4. Typical normalized PL spectra of the CdTe colloidal solution at different temperatures. The inset shows the shift of the luminescence peak (upper inset) and the temperature dependence of the Pl peak energy (lower inset) reprinted from [37].

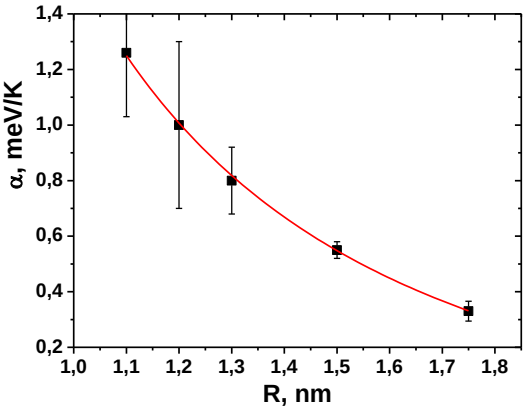

Fig. 5. The size dependence of the temperature sensitivity of CdTe quantum dots (the coefficient of determination is 0,99) reprinted from [37].

II-VI QDs lifetime luminescence thermometry

Due to the high temperature sensitivity of QDs Pl decay rate and high reading rate (hundreds of points per second) the lifetime luminescence technique is a very promising approach for high-resolution thermal imaging. Haro-González *et al.* [47] investigated the temperature dependence of CdTe QDs Pl lifetime in the biological range 20–50 ^{0}C. It has been shown that temperature sensitivity increases by more than one order of magnitude (from 0.0008 up to 0.017 °C^{-1}) when the QDs size decreases from 7,8 to 1 nm (Fig. 6). To demonstrate the potential of the practical application of lifetime based technique authors have determined the thermal loading caused by tightly focused laser beams in microfluidics.

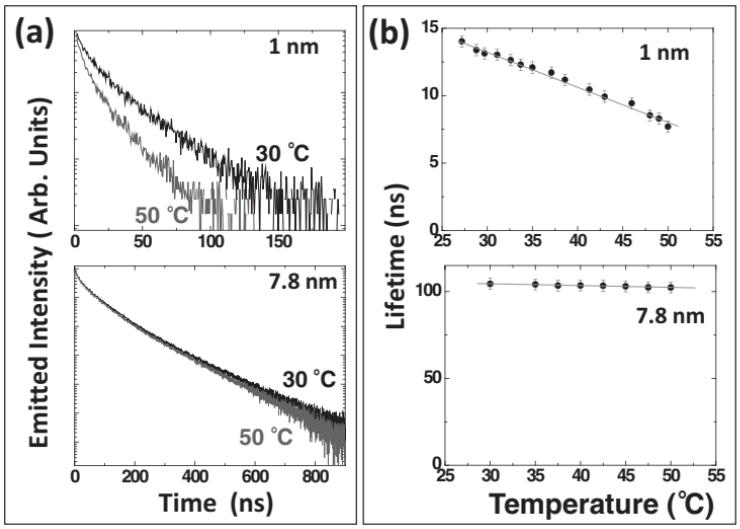

Fig. 6. Pl decay curves: a) and Pl lifetime; b) of 1 nm and 7,8 nm CdTe QD at different temperatures [47].

Experimental data showed good agreement with theoretically predicted values demonstrating the ability of CdTe-QDs as lifetime-based nanothermometers.

One of the most challenging tasks in QDs luminescent thermometry is the reversibility of the QDs temperature sensors. Chen *et al.* [48] studied the effect of cyclic heating and cooling on the luminescent parameters (Pl intensity and wavelength) of CdSe/ZnS QDs and their PMMA composites. It has been shown that in the temperature range of 27–115 ^{0}C the first four cycles decreased the maximum of Pl intensity corresponding to the temperature minimum when its minimum was relatively independent of the cycle number. This suggests that the heating partially damages the QDs surface when the cooling recovers it. At a temperature higher than 310 ^{0}C the QDs structures destroy completely leading to irreversible changes in Pl properties. Recently Zhang *et al.* [49] developed the highly stable low toxic CdTe/ZnS-SiO_2 core/shell nanocrystals exhibiting outstanding reversible linear temperature dependence of the Pl maximum in 22–80 ^{0}C temperature range. Obtaining the polymer films by spin coating of QDs dispersion with PDMS authors have demonstrated a very promising sensor for thermal monitoring of high-speed bearing rotating components, which has great potential for practical use.

I-III-VI QDs as temperature sensors

Even in the absence of excitonic emission I-III-VI QDs possess the temperature dependent on PL intensity, wavelength, and lifetime response, but its mechanism is still needed to be established. One of the explanations is that the thermally activated dissociation of metal-ligand complexes on the QDs surface is responsible for the Pl parameters changes during the heating-cooling of the system. As an example, Stroyuk *et al.* [50] reported a strong and reversible temperature dependence of the photoluminescence quantum yield and average PL lifetime of aqueous glutathione (GSH)-capped Ag−In−S and their core/shell AIS/ZnS heterostructures. Authors have shown that both core and core-shell QDs reveal strong PL quenching upon heating from 10 to 80 °C (Fig. 7a), which is completely reversible (Fig. 7b) upon cooling without any noticeable signs of aggregation of NPs or degradation of their emissive capacity. This observation indicates that Pl quenching is caused by the reversible process of activation/deactivation of some non-radiative relaxation pathways. Finally, it was assumed that these pathways emerge due to the thermally activated dissociation of metal-GSH complexes on the surface of the AIS NCs and the introduction of water molecules into the first coordination sphere favoring a non-radiative vibrational relaxation of the excitation energy.

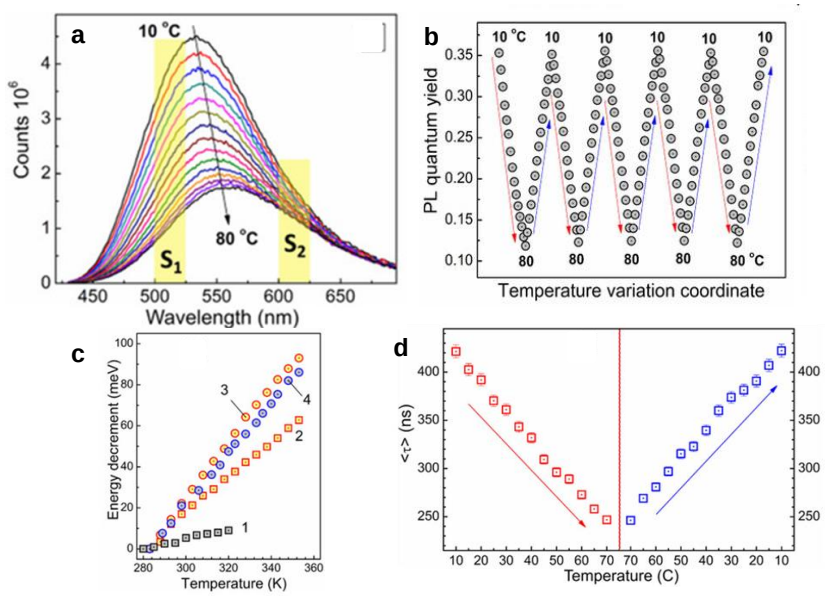

Fig. 7. a) Pl spectra of AIS nanocrystals at different temperatures; b) PL QY of AIS QDs with temperature changing cyclically; c) temperature dependences of the PL band maximum energy decrement of GSH-capped NC ensemble dried on a glass plate (1), dispersed in aqueous colloid (2), as well as a fraction of the smallest AIS QDs obtained via size selective precipitation (3) and aqueous PEI-capped CdS NCs (4); d) PL lifetime as a function of the temperature of AIS QDs solution in a regime of heating (red squares) and cooling (blue squares)(50).

The spectral position of Pl band of AIS NPs is also sensitive to temperature change shifting from 2.01 eV to 1.95 eV when temperature increase from 10 °C to 80 °C. This red shift of Pl wavelength is reversible as well and explained here mostly by a decrease of the spatial exciton confinement resulting from the thermally-activated dissociation of the surface Ag-GSH complexes, but a variation of the spatial exciton confinement arising from the thermal lattice expansion as well as the temperature dependence of the population of lattice defects and various recombination events are also not excluded. Other interesting observations are illustrated on Fig. 7c: first, the temperature sensitivity (slope of curves in coordinates "energy decrement – temperature") is higher for QDs dispersed in water in comparison with those dried on the glass substrate, and second, the smaller QDs are more sensitive to the temperature fluctuation that the bigger one (fraction of NPs with a different size was obtained here by size-selective precipitation). The first observation indicates that the mechanism of the temperature-induced changes of the PL parameters of AIS NPs is different for aqueous colloids and in the case of dried samples. The second one confirms that the temperature sensitivity of Pl band position of AIS QDs is size dependent, as was shown previously for the CdTe nanocrystals [37].

Matsuda *et al.* [51] demonstrated a clear correlation between the temperature sensitivity of ZAIS nanocrystals and their composition. Three samples of $ZAIS_x$ QDs with x ranging from 0,4 to 0,9 was synthesized and their Pl spectra were measured at 293–353 K

and an atmospheric pressure of 101 kPa. It was found that the temperature sensitivity of ZAIS decreased with increasing value of x (from – 1,15%/K at x = 0,4 to 0.92 %/K at x = 0,9) and is even higher than the temperature sensitivity of CdSe/ZnS (−0.63 %/K) [41]. It was also demonstrated that the temperature sensitivity is independent of the excitation wavelength. Since the Pl spectra position of ZAIS QDs is either not affected by the excitation wavelength it was assumed that the carriers recombination always occurs from the same excitation energy state and the thermal quenching of Pl is a nonradiative process from this energetically excited state. Redshifts of 0.12 ± 0.07 nm/K were observed in both ZAIS x=0.4 and ZAIS x=0.9 within the applied temperature range, and these values are comparable to previous studies of CdSe/ZnS wavelength sensitivity [32,41,46], which demonstrates the possibility to use ZAIS nanoparticles in spectral position thermometry. Moreover, it was also shown that the Pl parameters of ZAIS QDs are only slightly sensitive to the Oxygen pressure and these QDs possess higher photostability than CdSe/ZnS nanocrystals giving them more advantages for practical use.

The composition of $Zn_xAgInSe$ QDs also affects greatly on their temperature sensitivity [52]. With the increase in the Zn/Ag ratio from 0,3 to 1, the emission intensity increased, as well as the change in the intensity corresponding to a given change in the temperature, indicative of high-sensitivity temperature sensing. Direct correlation between Zn/Ag ratio and temperature sensitivity of Pl wavelength was also observed and explained by the decrease of Huang-Rhys factor indicative of the enhancement of the electron-phonon coupling of QDs with Zn/Ag ratio of 1.

Zhang *et al.* provided a great illustration of the application of CIS nanocrystals both in vivo and intracellular temperature sensing [53]. Firstly, the core–shell $CuInS_2$/ZnS QDs were prepared in organic solvent and the thermal sensitivity of Pl intensity was estimated (3.4 %/°C in n-hexan). Secondly, the QDs were encapsulated with polyoxyethylene stearate (PS) to obtain water-dispersible micelles. The temperature sensitivity of these QDs micelles decreased to 2.0%/°C; however, they proved to be resistant to environmental factors, such as ion concentration, pH, and protein concentration. The QD-micelles exhibit good reversibility without aggregation during repeated heating and cooling and only a little cytotoxic effect on HeLa and PC-3 cells. Moreover, the QD-micelle incorporated in cells showed good stability with preserving almost the same PL emission and temperature-sensitive characteristics in cells as in solution, which guaranteed accurate intracellular temperature sensing of individual cells (Fig. 8).

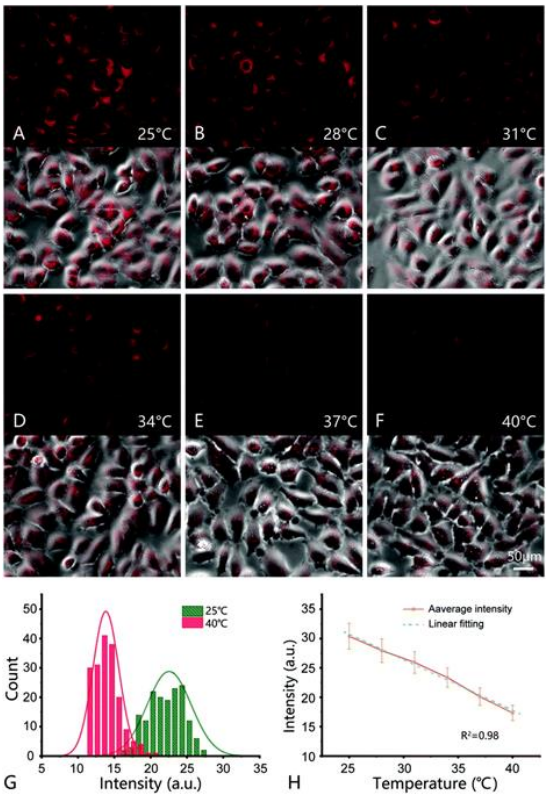

Fig. 8. (A–F) Fluorescence microscopy images and overlap images (DIC and fluorescence images) of HeLa cells in the temperature range of 25 °C to 40 °C labeled with QD-micelles. (G) Pl intensity distribution at different temperatures; (H) Cell average fluorescence intensity at different temperatures [53].

Meanwhile, the authors successfully applied QD-micelles to the thermometry of tumor tissues. The PL emission close to the near-infrared region has a good tissue penetration of excitation/emission light and a high signal-to-noise ratio. Live animal experiments showed that the PL intensity of tumor tissues injected with QD-micelles varies linearly with temperature over the physiological temperature range and the thermal sensitivity is similar to that in solution, proving its good stability in vivo. Therefore, these highly sensitive and highly stable NIR-emitting QD-micelles have considerable potential in biomedical applications.

Conclusions

Due to the size-, shape-, and composition-depended optical characteristics of semiconductor nanocrystals, they play an essential role in nanotechnology and are irreplaceable in many fields (electronics, LEDs, lasers, solar cells, and luminescent concentrators production, biosensor and bioimaging and so on).

Because of the high sensitivity of the QDs Pl parameters to the temperature fluctuations, they attract considerable attention as functional materials in the field of nanothermometry, providing high-resolution temperature profiles of micro-and photonic devices, where timely detecting of undesirable "hot spots" is very important to provide the

correct performance. On the other hand, many dynamic properties of biological systems as well as optical and structural properties of biomolecules are highly sensitive to even small temperature variations. In this case, a QDs nanothermometry is a very promising technic to detect cancer at an early stage when the number of cancer cells is about a thousand and the size of the tumor is yet invisible to traditional diagnostic methods (about 1 mm). Using QDs nanothermometers in biomedicine has an important advantage – they can be exited and detected within the biological optical window which provides the capability of deep tissue imaging.

Both II-VI and I-III-VI semiconductor nanocrystals have a high potential for practical use, the latter one, however, is more promising in terms of reduced toxicity and biocompatibility. The mechanisms of temperature response, in this case, are still under discussion as well as the origin of their luminescence, depending not only on the size, by from the composition of the nanocrystal.

From our point of view, the common issues restricting the mass implementation of these materials in the field of nanothermometry are related to the increase of reversibility and stability of Pl response under applied surrounding conditions, development of QDs materials with increased temperature sensitivity as well as improvement of procedures of utilization or excretion of QDs from the organism after being used.

Unified approach on how to evaluate, and report thermal sensitivity and which units to use has to be developed. The absence of it makes it difficult to compare the results of different authors and to rank the performance of different materials. However, a set of advantages inherent to this class of materials inspires a steady increase of works regarding QDs luminescent thermometry.

Acknowledgements

YK was partially supported by MESU [grant number 0123U100858]. YL and YK were supported by a grant from the Simons Foundation (Award Number: 1030286).

References

[1] Murray, C.B.; Norris, D.J.; Bawendi, M.G. Synthesis and characterization of nearly monodisperse CdE (E = sulfur, selenium, tellurium) semiconductor nanocrystallites. *J. Am. Chem. Soc.* **1993**, 115, 8706–8715. DOI: 10.1021/ja00072a025

[2] Pu, Y.; Cai, F.; Wang, D.; Wang, J.-X.; Chen, J.-F. Colloidal synthesis of semiconductor quantum dots toward large-scale production: a review. *Ind. Eng. Chem. Res.* **2018**, 57, 1790–1802. DOI: 10.1021/acs.iecr.7b04836

[3] De Arquer, F.P.G.; Talapin, D.V.; Klimov, V.I.; Arakawa, Y.; Bayer, M.; Sargent, E.H.; Baggiolini, A.; Callahan, S.J.; Luo, L.; Zuko, A.; et al. Semiconductor quantum dots: technological progress and future challenges. *Science* **2021**, 373, 8541. DOI: 10.1126/science.aaz8541

[4] Vu, T.Q.; Lam, W.Y.; Hatch, E.W.; Lidke, D.S. Quantum dots for quantitative imaging: from single molecules to tissue. *Cell Tissue Res.* **2015**, 360, 71–86. DOI: 10.1007/s00441-014-2087-2

[5] Resch-Genger, U.; Grabolle, M.; Cavaliere-Jaricot, S.; Nitschke, R.; Nann, T. Quantum dots versus organic dyes as fluorescent labels. *Nat. Methods* **2008**, 5, 763–775. DOI: 10.1038/nmeth.1248

[6] Cho, J.; Jung, Y.K.; Lee, J.-K. Kinetic studies on the formation of various II–VI semiconductor nanocrystals and synthesis of gradient alloy quantum dots emitting in the entire visible range. *J. Mater. Chem.* **2012**, 22, 10827–10833. DOI: 10.1039/C2JM16448E

[7] Yadav, A.N.; Singh, A.K.; Singh, K. Synthesis, properties, and applications of II–VI semiconductor core/shell quantum dots, in.: *Core/shell quantum dots*; (Eds.: Tong, X.M.; Wang Z.) **2020**, 1-28, Springer: Cham, Switzerland. DOI: 10.1007/978-3-030-46596-4_1

[8] Zhou, D.; Lin, M.; Chen. Z.; Sun, H.; Zhang, H.; Sun, H.; Yang, B. Simple synthesis of highly luminescent water-soluble CdTe quantum dots with controllable surface functionality. *Chem. Mater.* **2011**, 23, 4857–4862. DOI: 10.1021/cm202368w

[9] Subila, K.B.; Kumar, G.K.; Shivaprasad, S.M.; Thomas, K.G. Luminescence properties of CdSe quantum dots: role of crystal structure and surface composition. *J. Phys. Chem. Lett.* **2013**, 4, 2774–2779. DOI: 10.1021/jz401198e

[10] Nizamoglu, S.; Ozel, T.; Sari, E.; Demir, H.V. White light generation using CdSe/ZnS core-shell nanocrystals hybridized with InGaN/GaN light emitting diodes. *Nanotechnology* **2007**, 18, 065709. DOI: 10.1088/0957-4484/18/6/065709

[11] Tang, H.; Zhong, J.; Chen, W.; Shi, K.; Mei, G.; Zhang, Y.; Wen, Z.; Müller-Buschbaum, P.; Wu, D.; Wang, K.; Wei Sun, X. Lead sulfide quantum dot photodetector with enhanced responsivity through a two-step ligand-exchange method. *ACS Appl. Nano Mater.* **2019**, 2, 6135–6143. DOI: 10.1021/acsanm.9b00889

[12] Wu, R.; Wang, S.; Zhou, Y.; Long, J.; Dong, F.; Zhang, W. Chromium-based metal–organic framework MIL-101 decorated with CdS quantum dots for the photocatalytic synthesis of imines. *ACS Appl. Nano Mater.* **2019**, 2, 6818–6827. DOI: 10.1021/acsanm.9b01264

[13] Kokal, R.K.; Bredar, A.R.C.; Farnum, B.H.; Deepa, M. Solid-state succinonitrile/sulfide hole transport layer and carbon fabric counter electrode for a quantum dot solar cell. *ACS Appl. Nano Mater.* **2019**, 2, 7880–7887. DOI: 10.1021/acsanm.9b01264

[14] Bhandari, S.; Pramanik, S.; Biswas, N.K.; Roy, S.; Pan, U.N. Enhanced luminescence of a quantum dot complex following interaction with protein for applications in cellular imaging, sensing, and white-light generation. *ACS Appl. Nano Mater.* **2019**, 2, 2358–2366. DOI: 10.1021/acsanm.9b00233

[15] Xie, R.; Rutherford, M.; Peng, X. Formation of high-quality I–III–VI semiconductor nanocrystals by tuning relative reactivity of cationic precursors. *J. Am. Chem. Soc.* **2009**, 131, 5691–5697. DOI: 10.1021/ja9005767

[16] Regulacio, M.D.; Win, K.Y.; Lo, S.L.; Zhang, S.Y.; Zhang, X.; Wang, S.; Zheng, Y. Aqueous synthesis of highly luminescent $AgInS_2$–ZnS quantum dots and their biological applications. *Nanoscale* **2013**, 5, 2322–2327. DOI: 10.1039/C3NR34159C

[17] Soares, J.X.; Wegner, K.D.; Ribeiro, D.S.; Melo, A.; Häusler, I.; Santos, J.L.; Resch-Genger, U. Rationally designed synthesis of bright $AgInS_2$/ZnS quantum dots with emission control. *Nano Res.* **2020**, 13, 2438–2450. DOI: 10.1007/s12274-020-2876-8

[18] Kolny-Olesiak, J.; Weller, H. Synthesis and application of colloidal $CuInS_2$ semiconductor nanocrystals. *ACS Appl. Mater. Interfaces* **2013**, 5, 12221–12237. DOI: 10.1021/am404084d

[19] Park, S.H.; Hong, A.; Kim, J.-H.; Yang, H.; Lee, K.; Jang, H.S. Highly bright yellow-green-emitting $cuins_2$ colloidal quantum dots with core/shell/shell architecture for white light-emitting diodes. *ACS Appl. Mater. Interfaces* **2015**, 7, 6764–6771. DOI: 10.1021/acsami.5b00166

[20] Ruan, C.; Zhang, Y.; Lu, M.; Ji, C.; Sun, C.; Chen, X.; Chen, H.; Colvin, V.L.; Yu, W.W. White light-emitting diodes based on $AgInS_2$/ZnS quantum dots with improved bandwidth in visible light communication. *Nanomaterials* **2016**, 6, 13. DOI: 10.3390/nano6010013

[21] Lu, H.; Hu, Z.; Zhou, W.; Wie, J.; Zhang, W.; Xie, F.; Guo, R. Synthesis and structure design of I–III–VI quantum dots for white light-emitting diodes. *Mat. Chem. Front.* **2022**, 6, 418–429. DOI: 10.1039/D1QM01452H

[22] Ganguly, P.; Mathew, S.; Clarizia, L.; Kumar, R.S.; Akande, A.; Hinder, S.J.; Breen, A.; Pillai, S.C. Ternary metal chalcogenide heterostructure ($AgInS_2$–TiO_2) nanocomposites for visible light photocatalytic applications. *ACS Omega* **2020**, 5, 406–421. DOI: 10.1021/acsomega.9b02907

[23] Liu, S.; Na, W.; Pang, S.; Shi, F.; Su, X. A label-free fluorescence detection strategy for lysozyme assay using $CuInS_2$ quantum dots. *Analyst* **2014**, 139, 3048-3054. DOI: 10.1039/C4AN00160E

[24] Maji, S.K. Luminescence-tunable ZnS–$AgInS_2$ nanocrystals for cancer cell imaging and photodynamic therapy. *ACS Appl. Bio Mater.* **2022**, 5, 1230–1238. DOI: 10.1021/acsabm.1c01247

[25] Perner, V.; Rath, T.; Pirolt, F.; Glatter, O.; Wewerka, K.; Letofsky-Papst, I.; Zach, P.; Hobisch, M.; Kunert, B.; Trimmel, G. Hot injection synthesis of $CuInS_2$ nanocrystals using metal xanthates and their application in hybrid solar cells. *New J. Chem.* **2019**, 43, 356–363. DOI: 10.1039/C8NJ04823A

[26] Hashemkhani, M.; Loizidou, M.; MacRobert, A.J.; Yagci Acar, H. One-step aqueous synthesis of anionic and cationic $AgInS_2$ quantum dots and their utility in improving the efficacy of ALA-based photodynamic therapy. *Inorg. Chem.* **2022**, 61, 2846–2863. DOI: 10.1021/acs.inorgchem.1c03298

[27] Zhong, H.Z.; Zhou, Y.; Ye, M.F.; He, Y.J.; Ye, J.P.; He, C.; Yang, C.H.; Li, Y.F. Controlled synthesis and optical properties of colloidal ternary chalcogenide $CuInS_2$ nanocrystals. *Chem. Mater.* **2008**, 20, 6434–6443. DOI: 10.1021/cm8006827

[28] Li, X.; Tu, D.; Yu, S.; Song, X.; Lian, W.; Wei, J.; Shang, X.; Li, R.; Chen, X. Highly efficient luminescent I-III-VI semiconductor nanoprobes based on template-synthesized $CuInS_2$ nanocrystals. *Nano Res.* **2019**, 12, 1804–1809. DOI: 10.1007/s12274-019-2435-3

[29] Hamanaka, Y.; Ogawa, T.; Tsuzuki, M.; Kuzuya, T. Photoluminescence Properties and Its Origin of $AgInS_2$ Quantum Dots with Chalcopyrite Structure. *J. Phys. Chem. C* **2011**, 115, 1786–1792. DOI: 10.1021/jp110409q

[30] Valerini, D.; Cretí, A.; Lomascolo, M.; Manna, L.; Cingolani, R.; Anni, M. Temperature dependence of the photoluminescence properties of colloidal CdSe/ZnS core/shell quantum dots embedded in a polystyrene matrix. *Phys. Rev. B* **2005**, 71, 1–6. DOI: 10.1103/PhysRevB.71.235409

[31] Gaponenko, M.S.; Lutich, A.A.; Tolstik, N.A.; Onushchenko, A.A.; Malyarevich, A.M.; Petrov, E.P.; Yumashev, K.V. Temperature-dependent photoluminescence of PbS quantum dots in glass: evidence of exciton state splitting and carrier trapping. *Phys. Rev. B* **2010**, 82, 1–9. DOI: 10.1103/PhysRevB.82.125320

[32] Yu, H.C.Y.; Leon-Saval, S.G.; Argyros, A.; Barton, G,W. Temperature effects on emission of quantum dots embedded in polymethylmethacrylate. *Appl Opt.* **2010**, 49, 2749–2752. DOI: 10.1364/AO.49.002749

[33] Zhao, Y.; Riemersma, C.; Pietra, F.; Koole, R.; Donegá, C.D.M.; Meijerink, A. High-temperature luminescence quenching of colloidal quantum dots. *ACS Nano* **2012**, 6, 9058–9067. DOI: 10.1021/nn303217q

[34] Morello, G.; Giorgi, M.D.; Kudera, S.; Manna, L.; Cingolani, R.; Anni, M. Temperature and size dependence of nonradiative relaxation and exciton-phonon coupling in colloidal CdTe quantum dots. *J. Phys. Chem. C* **2007**, 111, 5846–5849. DOI: 10.1021/jp068307t

[35] Varshni, Y.P. Temperature dependence of the energy gap in semiconductors. *Physica* **1967**, 34, 149–154. DOI: 10.1016/0031-8914(67)90062-6

[36] Allahverdi, C.; Yükselici, M.H. Temperature dependence of absorption band edge of CdTe nanocrystals in glass. *New J. Phys.* **2008**, 10, 103029. DOI: 10.1088/1367-2630/10/10/103029

[37] Vyhnan, N.; Khalavka, Y. Size-dependent temperature sensitivity of photoluminescence peak position of CdTe quantum dots. *Luminescence* **2014**, 29, 952–954. DOI: 10.1002/bio.2600

[38] Joshi, A.; Narsingi, K.Y.; Manasreh, M.O.; Davis, E.A.; Weaver, B.D. Temperature dependence of the band gap of colloidal CdSe/ZnS core/shell nanocrystals embedded into an ultraviolet curable resin. *Appl. Phys. Lett.* **2006**, 89, 131907. DOI: 10.1063/1.2357856

[39] Murphy, G.P.; Zhang, X.; Bradley, A.L. Temperature-dependent luminescent decay properties of CdTe quantum dot monolayers: impact of concentration on carrier trapping. *J. Phys. Chem. C* **2016**, 120, 26490–26497. DOI: 10.1021/acs.jpcc.6b04734

[40] Jaque, D.; Vetrone, F. Luminescence nanothermometry. *Nanoscale* **2012**, 4, 4301. DOI: 10.1039/C2NR30764B

[41] Walker, G.W.; Sundar, V.C.; Rudzinski, C.M.; Wun, A.W.; Bawendi, M.G.; Nocera, D.G. Quantum-dot optical temperature probes. *Appl. Phys. Lett.* **2003**, 83, 3555–3557. DOI: 10.1063/1.1620686

[42] Han, B.; Hanson, W.L.; Bensalah, K.; Tuncel, A.; Stern, J.M.; Cadeddu, J.A. Development of quantum dot-mediated fluorescence thermometry for thermal therapies. *Ann. Biomed. Eng.* **2009**, 37, 1230–1239. DOI: 10.1007/s10439-009-9681-6

[43] Maestro, L.M.; Rodríguez, E.M.; Rodríguez, F.S.; De La Cruz, M.C.I.; Juarranz, A.; Naccache, R.; Vetrone, F.; Jaque, D.; Capobianco, J.A.; Solé, J.G. CdSe quantum dots for two-photon fluorescence thermal imaging. *Nano Lett.* **2010**, 10, 5109–5115. DOI: 10.1021/nl1036098

[44] Choudhury, D.; Jaque, D.; Rodenas, W.T.; Ramsey, T.; Paterson, L.; Kar, A.K. Quantum dot enabled thermal imaging of optofluidic devices. *Lab. Chip* **2012**, 12, 2414–2420. DOI: 10.1039/C2LC40181A

[45] Yang, J.; Ling, Z.; Li, B.Q.; Li, R.; Mei, X. Nanoscale 3D temperature gradient measurement based on fluorescence spectral characteristics of the CdTe quantum dot probe. *Opt. Express* **2019**, 27, 6770–6791. DOI: 10.1364/OE.27.006770

[46] Li, S.; Zhang, K.; Yang, J.M.; Lin, L.W.; Yang, H. Single quantum dots as local temperature markers. *Nano Lett.* **2007**, 7, 3102–3105. DOI: 10.1021/nl071606p

[47] Haro-González, P.; Martínez-Maestro, L.; Martín, I.R.; García-Solé, J.; Jaque, D. High-sensitivity fluorescence lifetime thermal sensing based on CdTe quantum dots. *Small* **2012**, 8, 2652–2658. DOI: 10.1002/smll.201102736

[48] Chen, Y.; Luan, W.; Zhang, S.; Yang, F. Quantum-dots based materials for temperature sensing: effect of cyclic heating-cooling on fluorescence. *J. Nanoparticle Res.* **2019**, 21, 185. DOI: 10.1007/s11051-019-4629-8

[49] Zhang, P.; Pan, A.; Yan, K.; Zhu, Y.; Hong, J.; Liang, P. High-efficient and reversible temperature sensor fabricated from highly luminescent CdTe/ZnS-SiO_2 nanocomposites for rolling bearings. *Sens. Actuators A Phys.* **2021**, 328, 112758. DOI: 10.1016/j.sna.2021.112758

[50] Stroyuk, O.; Raevskaya, A.; Spranger, F.; Gaponik, N.; Zahn, D.R.T. Temperature-dependent photoluminescence of silver-indium-sulfide nanocrystals in aqueous colloidal solutions. *ChemPhysChem* **2019**, 20, 1640–1648. DOI: 10.1002/cphc.201900088

[51] Matsuda, Y.; Torimoto, T.; Kameya, T.; Kameyama, T.; Kuwabata, S.; Yamaguchi, H.; Niimi, T. Zns-$AgInS_2$ nanoparticles as a temperature sensor. *Sens. Actuators B Chem.* **2013**, 176, 505–508. DOI: 10.1016/j.snb.2012.09.005

[52] Ding, Q.; Zhang, X.; Li, L.; Lou, X.; Xu, J.; Zhou, P.; Yan, M. Temperature dependent photoluminescence of composition tunable $Zn_{(x)}$AgInSe quantum dots and temperature sensor application. *Opt. Express* **2017**, 25, 19065–19076. DOI: 10.1364/OE.25.019065

[53] Zhang, H.; Wu, Y.; Gan, Z.; Yang, Y.; Liu, Y.; Tang, P. Wu, D. Accurate intracellular and in vivo temperature sensing based on $CuInS_2$/ZnS QD micelles. *J. Mater. Chem. B* **2019,** 7, 2835–2844. DOI: 10.1039/C8TB03261K